REALIZATION OF FLYBACK OPERATION IN DAB CONVERTER FOR INTEGRATED PV INVERTER AND BATTERY

S. Anusha[1], N. Arpana[2]

[1] *Student, Dept of EEE, Sahaja Institute of Technology & Sciences for Women, Telangana, India*
[2] *Asst.Prof, Dept of EEE, Sahaja Institute of Technology & Sciences for Women, Telangana, India*

ABSTRACT

This paper presents photovoltaic inverter with integrated battery storage used in Distribution power generation purpose. The dual active bridge topology was selected based on following specifications .Galvanic isolation Soft switching operation Simple phase shift power control. The dual active bridge with the storage for which it can be used transferred energy to other elements in the grid .A novel DAB switching scheme was introduced for ac –dc stage of module integrated power converters for PV applications. The modified flyback switching scheme exhibits 8% higher efficiency than DAB mode at 10 W, which comes at the cost of an additional switch. While flyback mode exhibits more core losses and slightly more conduction losses compared to DAB mode, the switching losses are significantly reduced by eliminating most of the switching actions and reducing the frequency. In addition, it was shown that the flyback mode achieves higher accuracy in power regulation for low-power levels compared to the DAB mode, resulting in a more stable operation and avoiding potential limit cycle oscillations. The proposed dual-mode control scheme is simulated using MATLAB software at low power.

Keyword: - *Dual active bridge (DAB), isolated dc–dc converter, photovoltaic (PV) inverters*

1. INTRODUCTION

The intermittent nature of PV and other renewable energy sources, and thus the need for energy storage and or load shedding, is a major challenge in small-scale PV-based power grids.[1,2,3]. This is despite power quality requirements. Low-power dc–dc micro converters and ac– dc (MIV) provide high-granularity maximum power point tracking (MPPT) at the module or substring level. This leads to increased robustness to clouds, dirt, and aging effects, as well as irradiance and temperature gradients. A conventional MIV-based ac power system with the energy storage system (ESS), which is definitely required for islanded operation on the scale of one or more houses, for example, is usually based on a high power centralized bidirectional ac–dc converter, which is interfaced to a battery bank or a flywheel is shown in fig 1[5]

Existing IV architectures satisfy the need for low capital cost and expandable ac generation, whereas there is a compelling argument to extend this technology to include small scale distributed storage. A novel topology with distributed storage is proposed for grid stabilization while potentially improving the generator lifetime and saving fuel. MIV integrated storage helps to buffer the frequent irradiance fluctuations while also providing local backup power and reactive power support.[8-9]

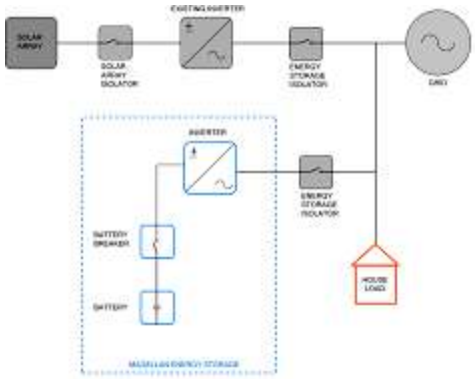

Fig-1: Conventional MIV-based PV system with a central ESS.

The general architecture of a two-stage MIV with an integrated ESS. While two-stage MIVs have a slightly lower efficiency than their single-stage counterparts, the high-voltage dc-link capacitance C_{bus} can be used for ac power decoupling in single-phase systems.[10]

This objective of this paper is to demonstrate a novel low power operating mode in dual active bridge converter, as well as dynamic dc link optimization scheme to maintain high efficiency over a broad power range and this work targets modular Nano grid for remote locations, where photovoltaic modules can be gradually introduced to grow the renewable energy at minimal cost, while reducing dc fuel consumption. Grid tide micro inverters provide a modular solution for ac power generation. The main contribution of this work is a new micro inverter platform and control scheme with bidirectional power flow between the Nano grid, the photovoltaic module and integrated short term storage, using high energy density Li-ion capacitor technology.[4]

The general architecture of a two-stage MIV with an integrated ESS is shown in Fig. 2. While two-stage MIVs have a slightly lower efficiency than their single-stage counterparts, the high-voltage dc-link capacitance C_{bus} can be used for ac power decoupling in single-phase systems [11], [13].

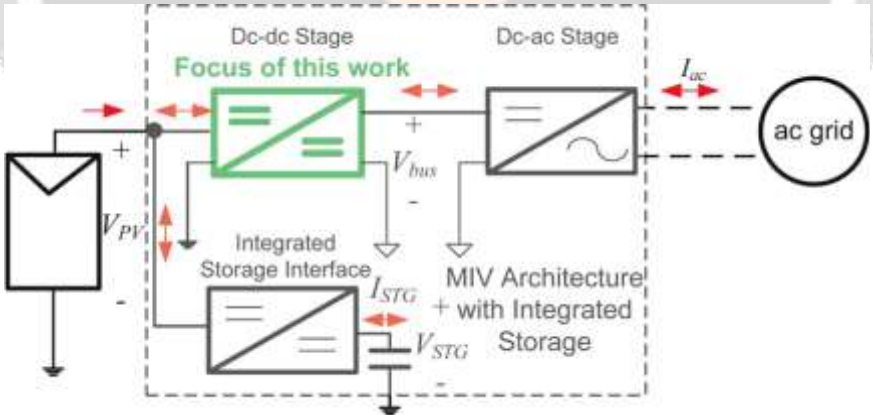

Fig-2: Two-stage IV architecture with integrated storage.

2. PROPOSED DAB ARCHITECTURE AND PRINCIPLE OF OPERATION

The proposed dc–dc architecture is shown in Fig. 3(a). This converter is a modified DAB that interfaces *V*PV with the dc link V_{bus}.

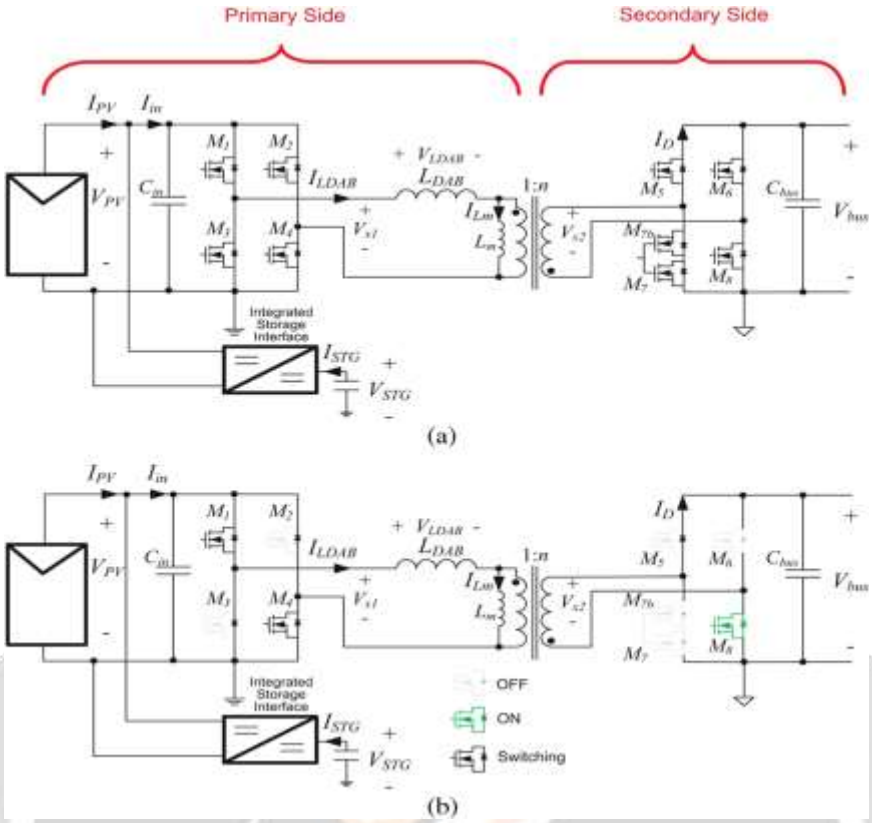

Fig-3: (a) Proposed modified DAB dc–dc architecture for improved low-power efficiency. (b) Switch configuration in flyback mode.

2.1 DAB Mode

The DAB topology was selected based on
1) Galvanic isolation,
2) soft-switching operation, and
3) Simple phase-shift power control [20], [21].
In addition, the DAB topology is bidirectional; therefore, the storage can be used to transfer energy to/from other elements in the grid. The average power from *V*PV to *V*bus, i.e., *P*, is

$$P = \frac{V_{\mathrm{PV}} V_{\mathrm{bus}}}{n\omega_s L_{\mathrm{DAB}}} \phi \left(1 - \frac{|\phi|}{\pi}\right) \qquad (1)$$

where *n* is the transformer's turns ratio; and *L*DAB is the DAB inductance, which is the sum of transformer's leakage inductance *L*leak and an optional external inductance *L*ext. φ is the phase shift between the two bridges, and $\omega s = 2\pi fs$, where *fs* is the switching frequency. The switching waveforms of the DAB converter are shown in Fig. 4(a). The slopes of the DAB inductance current *I*LDAB in switching states I and II are, respectively, calculated as

$$s_1 = \frac{V_{\mathrm{PV}} + \frac{V_{\mathrm{bus}}}{n}}{L_{\mathrm{DAB}}} \qquad (2)$$

$$s_2 = \frac{V_{\mathrm{PV}} - \frac{V_{\mathrm{bus}}}{n}}{L_{\mathrm{DAB}}}. \qquad (3)$$

In two-stage MIV architectures, *V*bus is generally regulated to a fixed voltage by the inverter stage. The reference voltage *V*bus is usually chosen to optimize efficiency at the nominal operating point [7]. It can be shown that the DAB converter achieves turn-on zero-voltage switching (ZVS) and maximum efficiency when *V*bus = *nV*PV, as the

reactive circulating current is minimized [20]. Meeting this condition leads to $s2 = 0$, thereby resulting in full free-wheeling in *I*LDAB during state II. In order to minimize the losses in the DAB, the reference for the dc-link voltage *V*bus is dynamically adjusted in the inverter stage such that *V*bus = *nV*MPP, where *V*MPP is the PV MPP voltage. It is well known that *V*MPP undergoes a relatively low fluctuation of about 30% during the course of a typical day [22]. This is in contrast to the PV current at MPP, i.e., *I*MPP, which is proportional to irradiance and thus has large-scale fluctuations, particularly on cloudy days.

2.2 Flyback Mode

A typical PV generator spends more than two thirds of the time operating below 50% of its rated power [7]. The conventional DAB converter suffers from relatively poor efficiency at low power due to high switching and drive losses [20], hence the need for a dedicated low-power mode. A general design method for DAB mode operation based on frequency optimization is introduced in [20

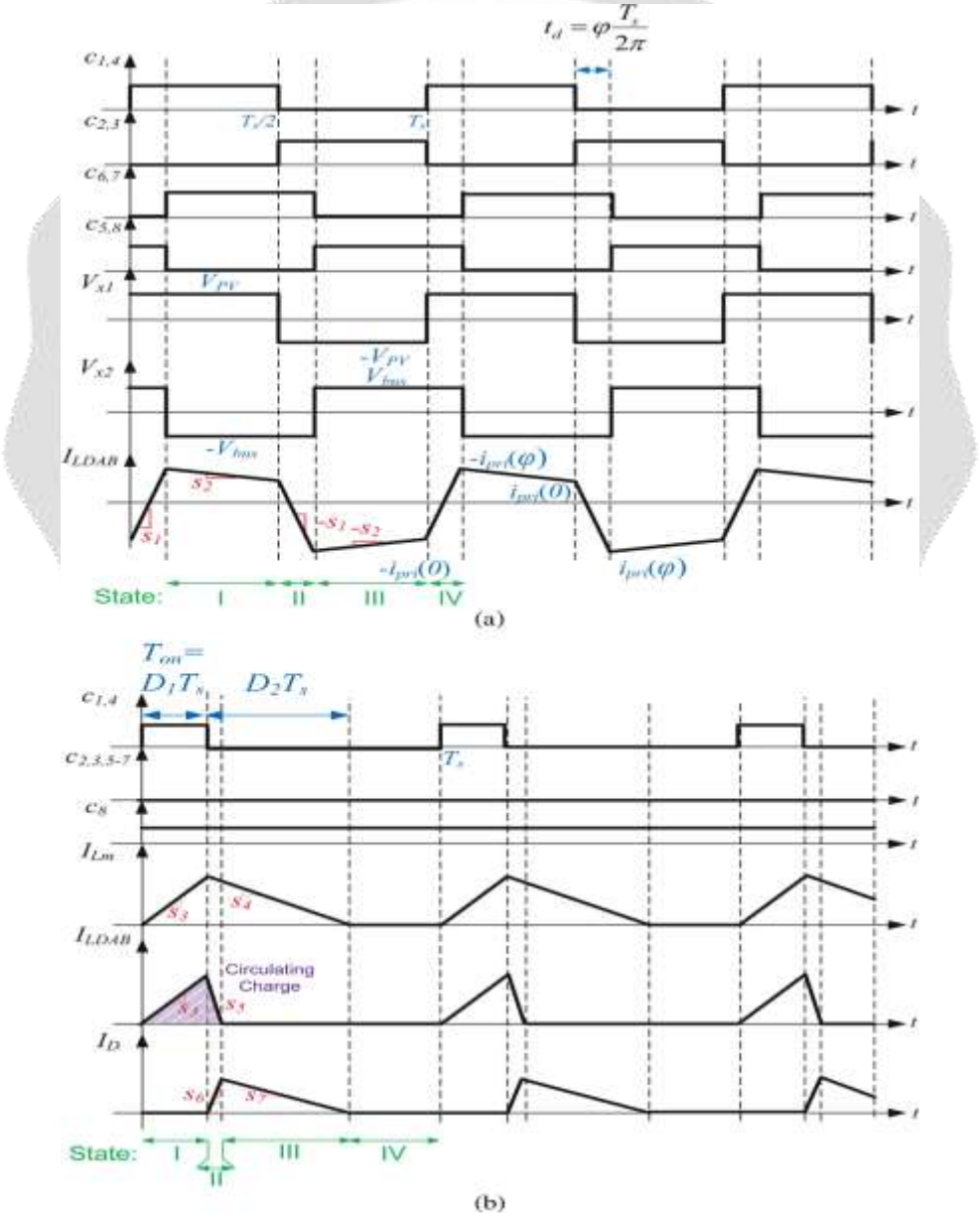

Fig-4: Switching waveforms in (a) DAB mode (b) Flyback mode

The DAB inductance circulates energy in every switching period in this mode. The rising slope of *I*LDAB is the same as *s*3, and the falling slope is

$$s_5 = \frac{-V_{\mathrm{PV}} - \frac{V_{\mathrm{bus}}}{n}}{L_{\mathrm{DAB}}}. \qquad (6)$$

Finally, the output diode current *ID* delivers charge to the bus with the following slopes in switching states II and III:

$$s_6 = \frac{s_4 - s_5}{n} \qquad (7)$$

$$s_7 = \frac{s_4}{n}. \qquad (8)$$

The 2T-flyback topology exhibits several advantages over DAB mode for low-power conditions, including lower switching and gate-driver losses (two switching devices versus nine in the DAB mode). Unlike the more conventional single-transistor flyback topology, the body diodes of *M*2 and *M*3 clamp the drain voltage on *M*1 and *M*4, which reduces electromagnetic interference and limits the blocking voltage rating on the primary switches to *V*PV. The flyback mode is operated with fixed on-time, i.e., *T*on, in pulse frequency modulation mode [26], where *T*on is given by

$$T_{\mathrm{on}} = D_1 T_s \qquad (9)$$

where *D*1 is the duty cycle in flyback mode, and *Ts* is the switching period. The corresponding converter waveforms are shown in Fig. 4(b). There are two inherent limitations to the 2T-flyback topology:

1) *D*1 must be less than 50% in order to avoid transformer saturation; and

2) *V*bus must be less than *nV*PV to ensure that the body diode of *M*5 transfers power to *V*bus when the primary-side switches are *off*. As a result, *V*bus needs to be reduced in flyback mode. The presence of *L*DAB, which is not required in the 2T-flyback topology, results in additional losses, since it circulates current in a switching period. The energy captured in *L*DAB is transferred back to the input capacitance *C*in in the 2T-flyback topology, as opposed to a conventional flyback scheme, which does not provide a return path for the energy absorbed by the leakage inductance. In addition, *L*DAB results in the soft turn-on of the output diode. The flyback mode exhibits unidirectional power transfer. The converter can operate with reverse power flow by adding another switch on the primary side. This additional switch is not included in the experimental prototype, as the efficiency in DAB mode is sensitive to conduction losses at the low-voltage high-current primary side. While possible, reverse power capability is not strictly needed in low-power flyback mode; the DAB can be prevented from operating in this condition by adopting burst-mode control instead, albeit at slightly lower efficiency than flyback mode.

3. DUAL-MODE CONTROL

The conceptual control diagram of the converter is shown in Fig. 5. c_{1-8} denote the gating voltages for switches *M*1−8. The DAB mode is adopted if *P* is higher than a threshold value P_{thresh} or if *P* is negative, in which case the storage is charged directly from the bus. In DAB mode, φ is controlled to regulate the power flow to/from the dc–ac stage, whereas the storage element's state-of-charge and MPPT operation can be controlled by the dedicated interface converter.

In flyback mode, *Ts* is adjusted by the controller *Gc*2(*s*), in order to regulate *P* to *P*. Assuming that the magnetizing inductance of the transformer, i.e., *Lm*, is much larger than *L*DAB, the power flow is given by

$$P = \frac{(V_{\mathrm{PV}} D_1)^2 T_s}{2L_m}. \qquad (10)$$

4. RESULTS AND ANALYSIS

The Simulation of the proposed system using MATLAB is shown in figures from 6 to 15. It is observed that proposed system is more efficient for both high efficiency and low efficiency applications as DAB and Flyback modes.

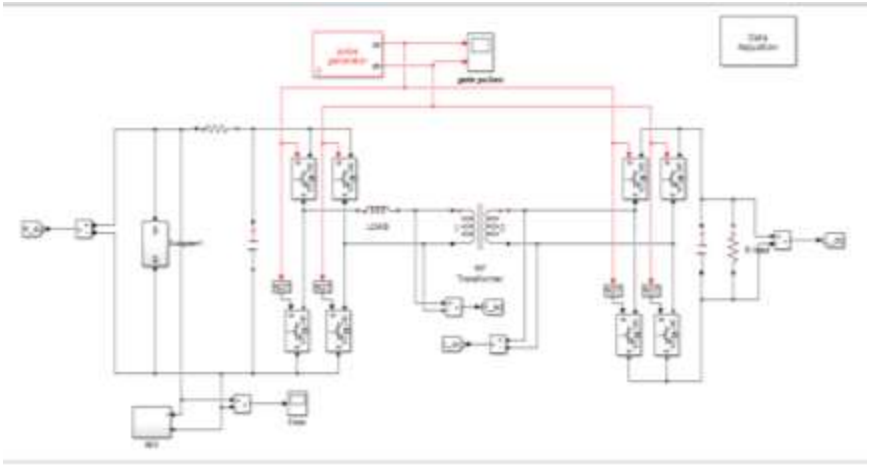

Fig-6: Simulation design of the proposed circuit using MATLAB

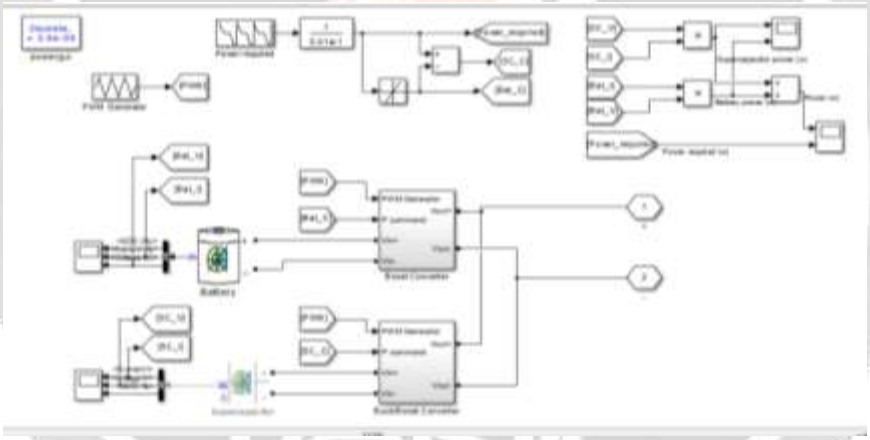

Fig-7: Integrated storage system design and its control

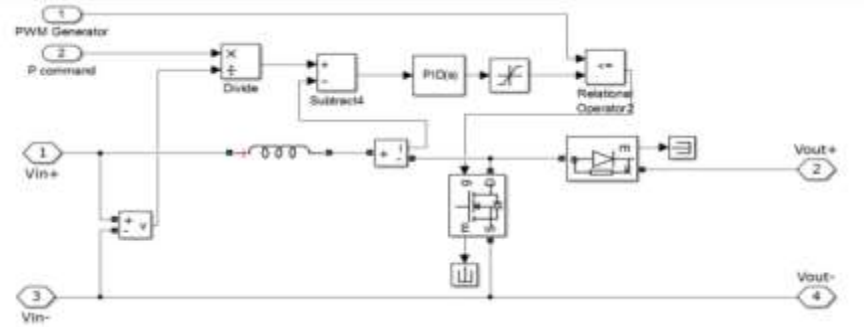

Fig-8: Buck/Boost control of proposed circuit

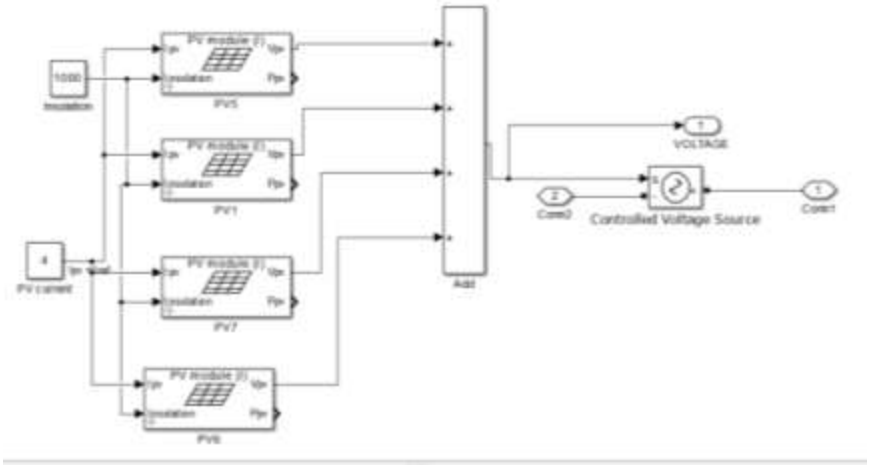

Fig-9: PV power stack system

4.1 DAB Mode

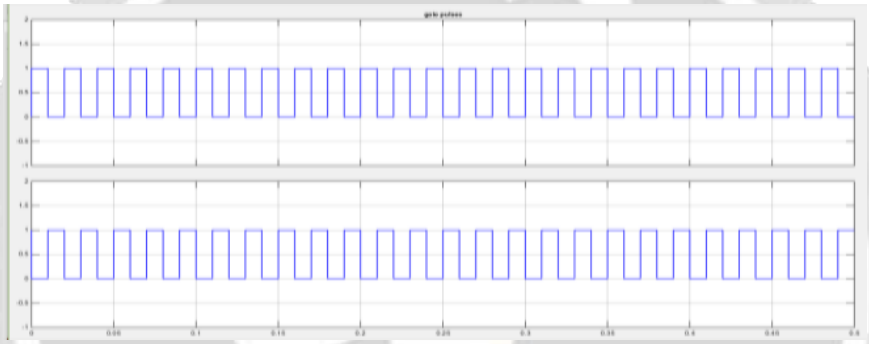

Fig-10: PWM pulses for DAB

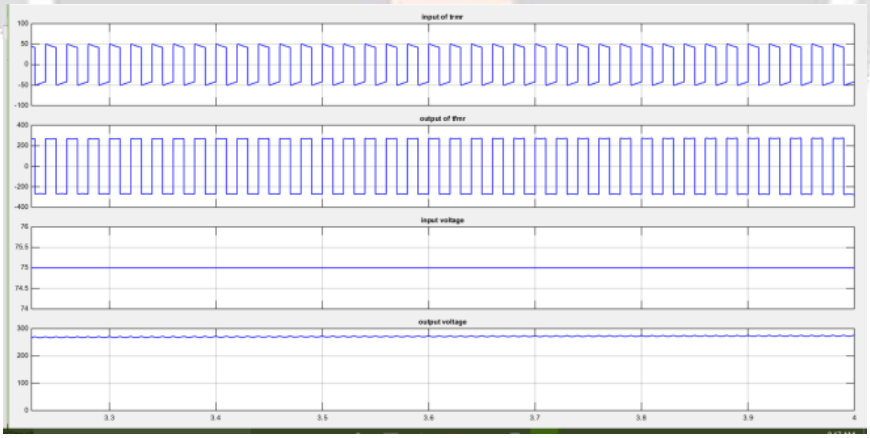

Fig-11: Input and output DC and AC quantities

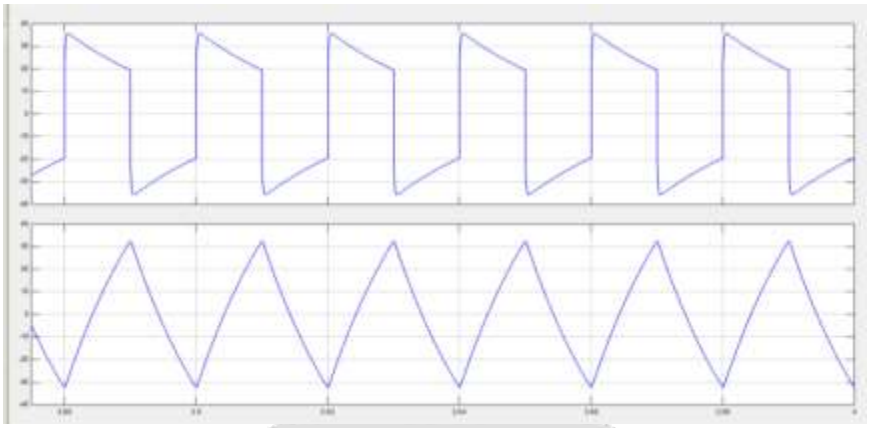

Fig-12: Voltage across and current through the switch

4.2 Flyback Mode

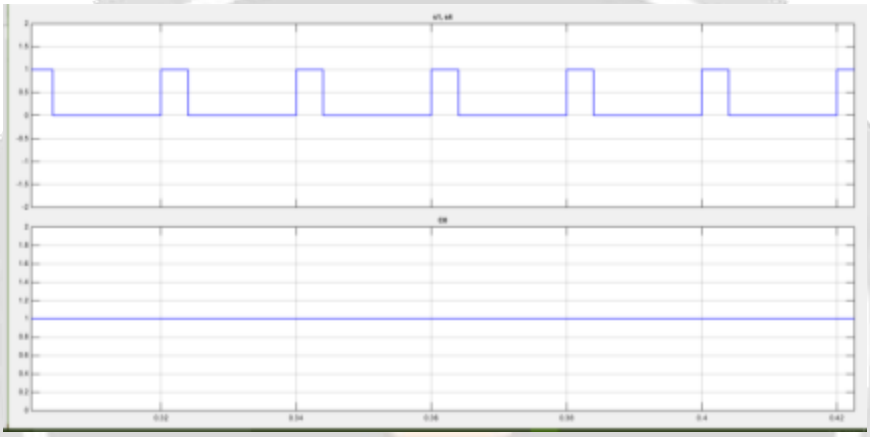

Fig-13: Gate pulse for flyback mode for 1,4 and 8 switches

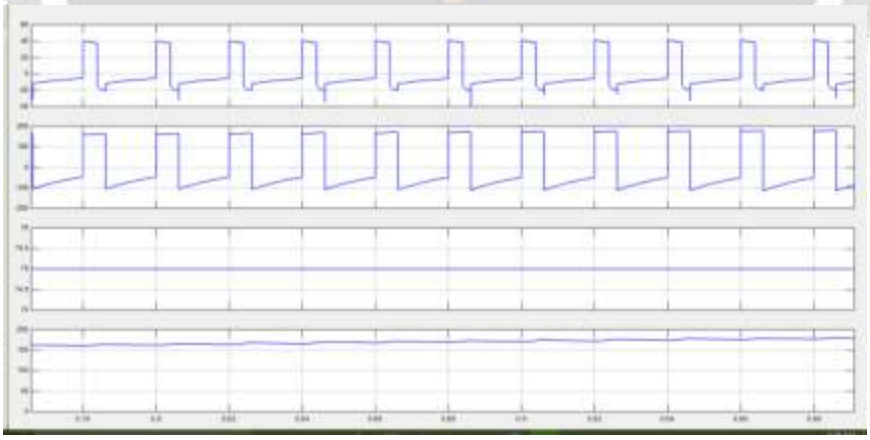

Fig-14: Voltage across Transformer and Input/output Voltages

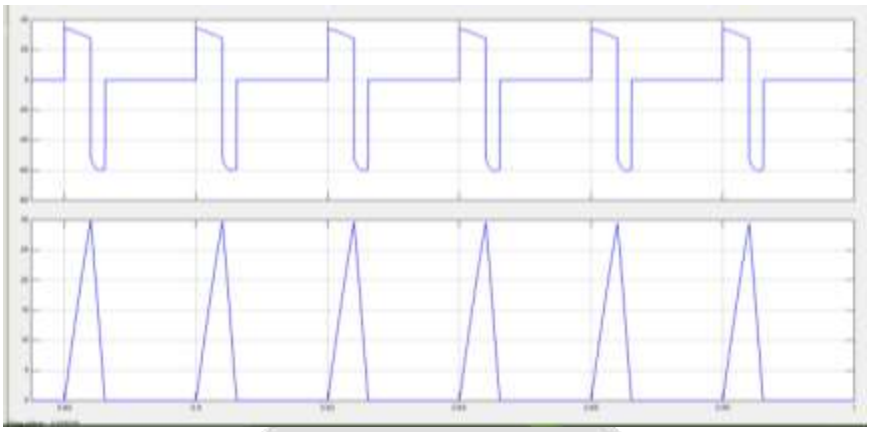

Fig-15: Voltage across and current through the switch

5. CONCLUSION

A novel DAB switching scheme was introduced for the dc–dc stage of module integrated power converters for PV applications. The modified flyback switching scheme exhibits 8% higher efficiency than DAB mode at 10 W, which comes at the cost of an additional switch. While flyback mode exhibits more core losses and slightly more conduction losses compared to DAB mode, the switching losses are significantly reduced by eliminating most of the switching actions and reducing the frequency. In addition, it was shown that the flyback mode achieves higher accuracy in power regulation for low-power levels compared to the DAB mode, resulting in a more stable operation and avoiding potential limit cycle oscillations.

6. REFERENCES

[1] R. Cabraal, "Experiences and lessons from 15 years of world bank sup-port for photovoltaics for off-grid electrification," in *Proc. 2nd ICDRET*, Jan. 2012, pp. 1–4.

[2] R. K. Hester *et al*., "High efficiency wide load range buck/boost/bridge photovoltaic micro converter," in *Proc. IEEE Appl. Power Electron. Conf. Expo.*, 2011, pp. 309–313.

[3] B. York, W. Yu, and J.-S. Lai, "An integrated boost resonant converter for photovoltaic applications," *IEEE Trans. Power Electron.*, vol. 28, no. 3, pp 199–1207, Mar. 2013.
pp. R. Erickson and A. Rogers, "A microinverter for building-integrated photovoltaics," in *Proc. IEEE Appl. Power Electron. Conf. Expo.*, 2009, 911–917.

[4] "Emphases m190 microninveter," Enphase Datasheet, 2009. [Online]. Available: http://enphaseenergy.com

[5] N. Femia, G. Lisi, G. Petrone, G. Spagnuolo, and M. Vitelli, "Dis-tributed maximum power point tracking of photovoltaic arrays: Novel approach and system analysis," *IEEE Trans. Ind. Electron.*, vol. 55, no. 7, pp. 2610–2621, Jul. 2008.

[6] S. Poshtkouhi, V. Palaniappan, M. Fard, and O. Trescases, "A general ap-proach for quantifying the benefit of distributed power electronics for fine grained MPPT in photovoltaic applications using 3-D modeling," *IEEE Trans. Power Electron.*, vol. 27, no. 11, pp. 4656–4666, Nov. 2012.

[7] L. Xu and D. Chen, "Control and operation of a dc microgrid with variable generation and energy storage," *IEEE Trans. Power Del.*, vol. 26, no. 4, pp. 2513–2522, Oct. 2011.

[8] G. Suvire, M. Molina, and P. Mercado, "Improving the integration of wind power generation into ac microgrids using flywheel energy storage," *IEEE Trans. Smart Grid*, vol. 3, no. 4, pp. 1945–1954, Dec. 2012.

[9] S. Poshtkouhi *et al*., "A dual-active-bridge based bi-directional micro-inverter with integrated short-term Li-ion ultra-capacitor storage and ac-tive power smoothing for modular PV systems," in *Proc. 29th Annu. IEEE APEC Expo.*, Mar. 2014, pp. 643–649.

[10] M. Alam, K. Muttaqi, and D. Sutanto, "Mitigation of rooftop solar PV impacts and evening peak support by managing available capacity of distributed energy storage systems," *IEEE Trans. Power Syst.*, vol. 28, no. 4, pp. 3874–3884, Nov. 2013.

[11] L. Liu, H. Li, Z. Wu, and Y. Zhou, "A cascaded photovoltaic system inte-grating segmented energy storages with self-regulating power allocation control and wide range reactive power compensation," *IEEE Trans. Power Electron.*, vol. 26, no. 12, pp. 3545–3559, Dec. 2011.

[12] Y.-M. Chen, A. Huang, and X. Yu, "A high step-up three-port DC–DC converter for stand-alone PV/battery power systems," *IEEE Trans. Power Electron.*, vol. 28, no. 11, pp. 5049–5062, Nov. 2013